

Achieving Organic Solar Cells with efficiency over 14% based on a non-Fullerene Acceptor incorporating the Cyclopentathiophene unit Fused backbone

Yao Cai,^{‡a} Lingxian Meng,^{‡a} Huanhuan Gao,^a Ziqi Guo,^a Nan Zheng,^b Zengqi Xie,^b Hongtao Zhang, Chenxi Li,^a Xiangjian Wan^{*a} and Yongsheng Chen^a

- a. The Centre of Nanoscale Science and Technology and Key Laboratory of Functional Polymer Materials, Institute of Polymer Chemistry, College of Chemistry, State Key Laboratory of Elemento-Organic Chemistry, Renewable Energy Conversion and Storage Center (RECAST), Nankai University, Tianjin 300071, China.*
- b. Institute of Polymer Optoelectronic Materials and Devices State Key Laboratory of Luminescent Materials and Devices South China University of Technology Guangzhou 510640, China*

Content

1. Materials and Synthesis
2. Measurements and Instruments
3. NMR and Mass Spectra
4. TGA Analysis and UV Absorption
5. Device Fabrication and Measurements
6. Reference

1. Materials and Synthesis

PBDB-T was purchased from 1-Material Inc. 1,8-diiodooctane (DIO) and MoO₃ were purchased from Alfa-Aesar. PFN-Br, i.e. poly[(9,9-bis{30-[N,N-dimethyl]-N-ethyl-ammonium}propyl)-2,7-fluorene)-alt-1,4 phenylene]dibromide was purchased from Luminescence Technology Corp. All other materials were purchased and used as received. Tetrahydrofuran (THF) and toluene were distilled from sodium benzophenone before use, and 1,2-dichloroethane was dried with calcium hydride.

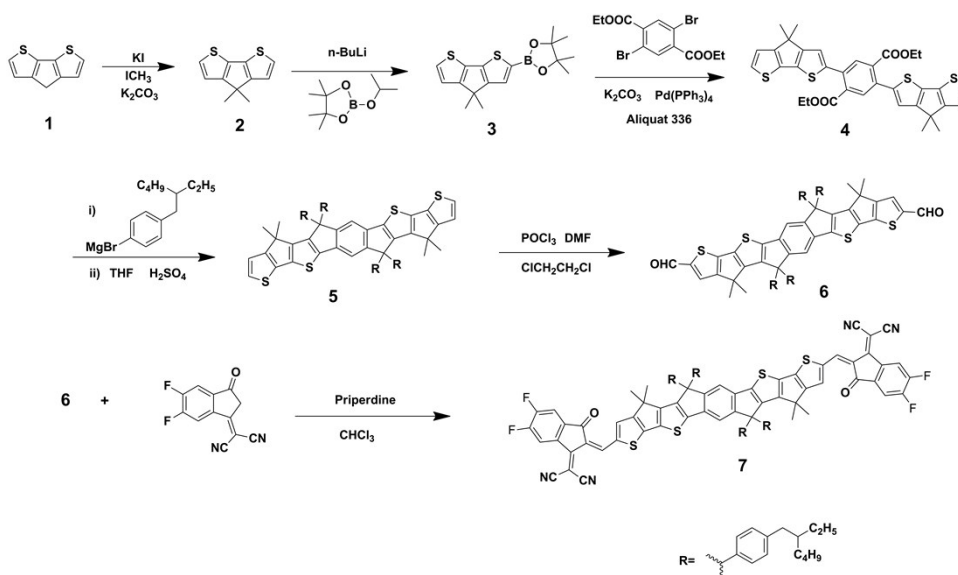


Figure S1 Synthetic route for BCPT-4F

Synthesis of 4,4-dimethyl-4H-cyclopenta[1,2-b:5,4-b'] dithiophene (compound 2)

To a solution of 4H-cyclopenta[1,2-b:5,4-b'] dithiophene (4.00 g, 22.44 mmol), potassium iodide (KI, 0.31 g, 1.88 mmol), potassium hydroxide (KOH, 4.44 g, 79.13 mmol) in DMSO (50mL) was added at room temperature with iodomethane (6.64 mL, 53.33 mmol) under nitrogen. The reaction mixture was stirred at room temperature overnight. Then the reaction mixture was extracted with ether and washed several times with water to decrease the amount of DMSO in organic phase. Then combined organic phases were dried over MgSO₄, evaporated and purified by flash chromatography on silica gel with hexane as an eluent. The title compound was obtained as yellow oil (4.13 g, 89%). ¹H NMR (400 MHz, CDCl₃, δ): 7.19(d, *J* = 4.9 Hz, 2H), 7.03(d, *J* = 4.9 Hz, 2H), 1.50(s, 6H).

Synthesis of 2-(4,4-dimethyl-4H-cyclopenta[1,2-b:5,4-b'] dithiophen-2-yl)-4,4,5,5-tetramethyl-1,3,2-dioxaborolane (compound 3)

In a 250mL round-bottomed flask, compound 2 (1.5 g, 7.27 mmol) was dissolved by 80mL tetrahydrofuran (THF) under nitrogen atmosphere. Then the solution was cooled to -40°C by an acetone/dry ice bath. N-Butyllithium (n-BuLi) in n-hexane (2.4 M, 3.03 mL, 7.27 mmol) was added to the mixture dropwise. After stirring 1.5 h at -40 °C, 1.95 mL 2-isopropoxy-4,4,5,5-tetramethyl-1,3,2-dioxaborolane was added in one portion, and stirred another 0.5 h at -40 °C. Then the mixture was

warmed up to room temperature and stirred overnight. After the reaction, the mixture was quenched with water and extracted with dichloromethane. The dichloromethane solution was dried over sodium sulfate and the solvent was removed by rotavapor. The crude product was directly subjected to the next reaction without further purification.

Synthesis of diethyl 2,5-bis(4,4-dimethyl-4H-cyclopenta[1,2-b:5,4-b']dithiophen-2-yl)terephthalate (compound 4)

The crude production of compound 3 in the above step was transferred to a 100 mL round-bottomed flask, then diethyl 2,5-dibromoterephthalate (793 mg, 2.09 mmol), K₂CO₃ (1.5 g, 10.98 mmol), methyl trioctyl ammonium chloride (218 mg, 0.54 mmol), Pd(PPh₃)₄ (171 mg, 0.15 mmol) were added to the reaction flask. Under nitrogen atmosphere, 50mL toluene and 10 mL H₂O were added, and the reaction was refluxed overnight. After reaction, 50mL dichloromethane was added. The mixture was washed with water (3×100mL) and the organic phase was separated and dried with anhydrous Na₂SO₄. The solvent was evaporated and the residue was purified by flash chromatography on silica gel. The final product was obtained as yellow solid (1.23 g, 93%). ¹H NMR (400 MHz, CDCl₃, δ): 7.81 (s, 2H), 7.20 (d, *J* = 4.9 Hz, 2H), 7.02 (s, 2H), 7.01 (d, *J* = 4.9 Hz, 2H), 4.25 (q, *J* = 7.1 Hz, 4H), 1.48 (s, 12H), 1.16 (t, *J* = 7.1 Hz, 6H). ¹³C NMR (101 MHz, CDCl₃) δ 168.40, 160.84, 160.50, 140.19, 136.70, 135.21, 133.71, 133.09, 131.25, 125.76, 120.91, 61.78, 53.49, 45.26, 25.14, 13.92.

Synthesis of compound 5

1-bromo-4-(2-ethylhexyl) benzene (2.15 g, 8 mmol) was added to 20 mL THF in a 100mL flask under nitrogen atmosphere. The mixture was cooled to -78 °C, and 2.7 mL n-BuLi (2.4 M, 6.36 mmol) was added dropwise. After addition, the mixture was stirred at -78 °C for 1.5 h. Then compound 3 was dissolved (0.5g, 0.79 mmol) in THF (3mL), and added it to the mixture dropwise slowly. After stirring for another 0.5h under -78°C, the mixture was warmed to room temperature and stirred overnight. Then, the mixture was quenched with water and extracted with dichloromethane. After drying with anhydrous Na₂SO₄, the solvent was evaporated and the residue was dissolved in 30 mL THF and heated to 50 °C. Concentrated H₂SO₄ (1mL) was added slowly to the above mixture. The mixture was heated and refluxed for 0.5 h. then quenched by water. Then, the mixture was quenched with water and extracted with dichloromethane. After drying with anhydrous Na₂SO₄, the solvent was evaporated and the residue was purified by flash chromatography using petroleum ether as fluent. The product was obtained as a yellow solid (0.48 g, 48%). ¹H NMR (400 MHz, CDCl₃, δ): 7.29 (d, *J* = 8.1 Hz, 5H), 7.28 (d, *J* = 7.1 Hz, 5H), 7.09 (d, *J* = 4.8 Hz, 2H), 7.04 (d, *J* = 8.1 Hz, 8H), 6.84 (d, *J* = 4.8 Hz, 2H), 2.46 (d, *J* = 6.7 Hz, 8H), 1.56 – 1.36 (m, 12H), 1.18 (m, 40H), 0.81 (m, 20H). ¹³C NMR (101 MHz, CDCl₃) δ 160.95, 156.29, 154.32, 151.49, 142.34, 140.63, 139.74, 138.32, 135.16, 124.67, 120.66, 114.71, 62.87, 45.94, 40.98, 39.64, 32.30, 28.84, 25.43, 24.09, 23.04, 14.17, 10.82.

Synthesis of compound 6

N, N-Dimethylformamide (5 mL) was added to a 50mL round-bottomed flask, and 2 mL phosphoryl trichloride was dropped slowly at 0 °C under nitrogen atmosphere. After stirred for 3 h at room temperature, the mixture was added to the solution of compound 5 (300 mg, 0.24 mmol) in dry 30mL 1,2-dichloroethane slowly. Then the mixture was refluxed under nitrogen overnight. After quenched by saturated sodium acetate solution. The mixture was extracted with dichloromethane. After drying with anhydrous Na₂SO₄, the organic solvent was evaporated and the residue was purified by flash chromatography (dichloromethane:petroleum ether, 1:1) afforded the product as an orange solid (276 mg, 87%). ¹H NMR (400 MHz, CDCl₂, δ): 9.75 (s, 2H), 7.43 (s, 2H), 7.33 (s, 2H), 7.25 (d, *J* = 7.8 Hz, 8H), 7.07 (d, *J* = 7.8 Hz, 8H), 2.57 (t, *J* = 7.4 Hz, 8H), 1.56 (m, 12H), 1.26 (m, 40H), 0.86(m, 20H). ¹³C NMR (101 MHz, CDCl₃, δ): 182.22, 160.92, 158.34, 157.09, 151.73, 147.16, 146.22, 143.02, 141.14, 138.93, 137.58, 135.55, 115.49, 62.95, 46.27, 40.95, 39.59, 32.24, 28.79, 25.40, 23.82, 23.00, 14.14, 10.79.

Synthesis of compound BCPT-4F

Compound 6 (100 mg, 0.08 mmol) was dissolved in 30mL dry chloroform in a 100 mL round-bottomed flask, then 2-(5,6-difluoro-3-oxo-2,3-dihydro-1H-inden-1-ylidene) malononitrile (183mg, 0.78 mmol) and 0.3 mL pyridine were added and stirred overnight at 30 °C. After the reaction, the organic phase was washed with water (3×50mL). The organic phase was separated and dried with Na₂SO₄. After removal of the solvent, the crude product was purified on a silica-gel column chromatography (dichloromethane:petroleum ether, 1:1). The pure product BCPT-4F was a black solid (103 mg, 75%). ¹H NMR (400 MHz, CD₂Cl₂, δ): 8.82 (s, 2H), 8.71 (s, 2H), 7.85 (s, 2H), 7.48 (s, 2H), 7.43 (s, 2H), 7.25 (d, *J* = 9.2 Hz, 8H), 7.09 (d, *J* = 8.2 Hz, 8H), 2.50 (t, *J* = 10.6 Hz, 8H), 1.63 – 1.37 (m, 6H), 1.27 (m, 46H), 1.06 – 0.69 (m, 24H). ¹³C NMR (101 MHz, CDCl₃, δ):185.10, 161.74, 160.76, 157.29, 156.95, 154.32, 151.74, 151.36, 140.52, 138.04, 137.21, 136.92, 136.56, 136.29, 135.50, 135.49, 135.06, 133.24, 128.26, 127.61, 117.43, 115.27, 113.90, 113.71, 111.12, 66.01, 62.00, 59.37, 45.18, 39.91, 38.56, 31.21, 28.68, 27.74, 24.39, 22.87, 21.96, 13.14, 9.76. HR-FTMS: calculated for C₁₁₂H₁₀₆F₄N₄O₂S₄ [M⁺], 1743.7168; found: 1744.7244.

2. Measurements and Instruments

¹H, ¹³C NMR spectra were measured in CDCl₃ using a Bruker AV400 Spectrometer. Fourier transform mass spectrometry (FTMS) with high resolution matrix assisted laser desorption/ionization (HR-MALDI) were performed on a Varian 7.0T FTMS instrument. Ultraviolet-visible (UV-Vis) absorption spectra were measured on a UV-Vis instrument Agilent Cary 5000 UV-vis-NIR spectrophotometer. A TA instrument NETZSCHSTA 409PC was performed to carry out thermogravimetric analyses (TGA) with heating rate of 10 °C·min⁻¹ under

nitrogen gas flow. UV-vis spectra were obtained with a JASCO V-570 spectrophotometer. Cyclic voltammetry (CV) experiments were employed to evaluate the energy levels with a LK98B II Microcomputer based Electrochemical Analyzer in dichloromethane solutions at room temperature. The experiments were carried out in a conventional three-electrode configuration with a saturated calomel electrode (SCE) as the reference electrode and a Pt wire as the counter electrode. Tetrabutylammonium phosphorus hexafluoride (Bu_4NPF_6 , 0.1 M) in dry dichloromethane was used as the supporting electrolyte with the scan rate of 100 mVs^{-1} under the protection of nitrogen. The energy levels were calculated by the use of versatile calculation formula (assumed the energy level of $\text{FeCp}_2^{+/0}$ to be 4.8 eV below vacuum): $E_{\text{HOMO}} = -e[\text{E}_{\text{OX}} + (4.8 - E_{\text{Fc}})]\text{eV}$; $E_{\text{LUMO}} = -e[\text{E}_{\text{red}} + (4.8 - E_{\text{Fc}})]\text{eV}$.

3. NMR and Mass Spectra

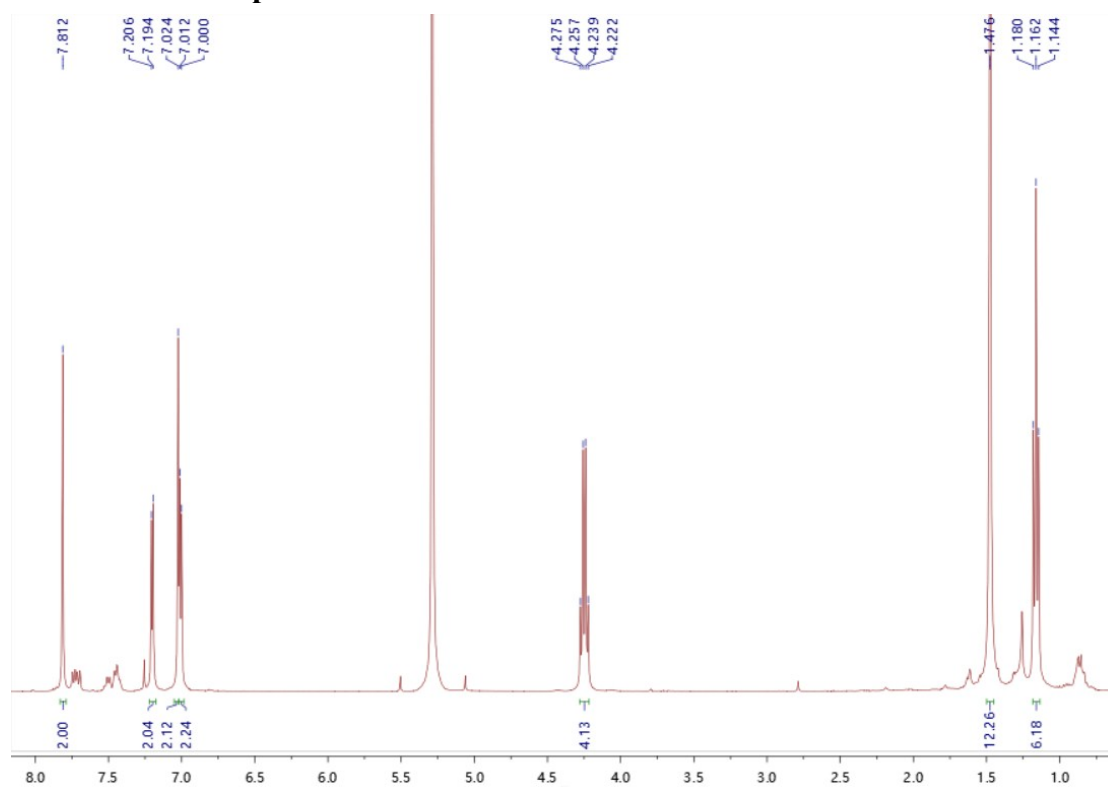


Figure S2. ^1H NMR of Compound 4

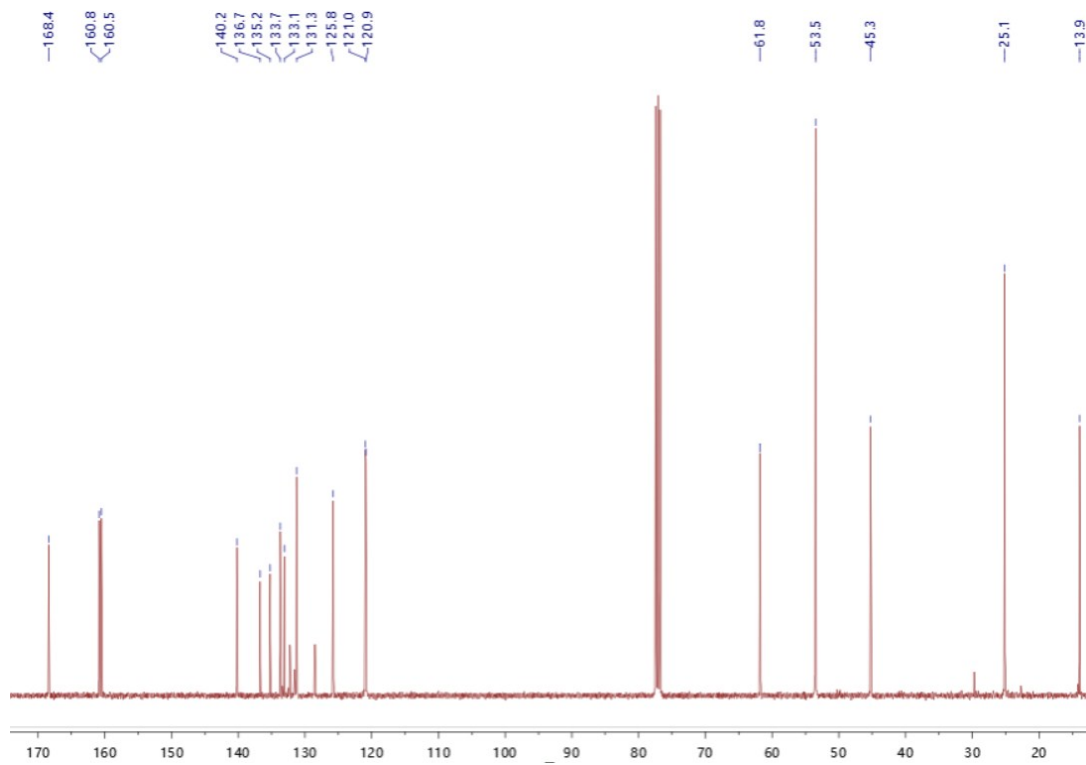


Figure S3. ^{13}C NMR of Compound 4

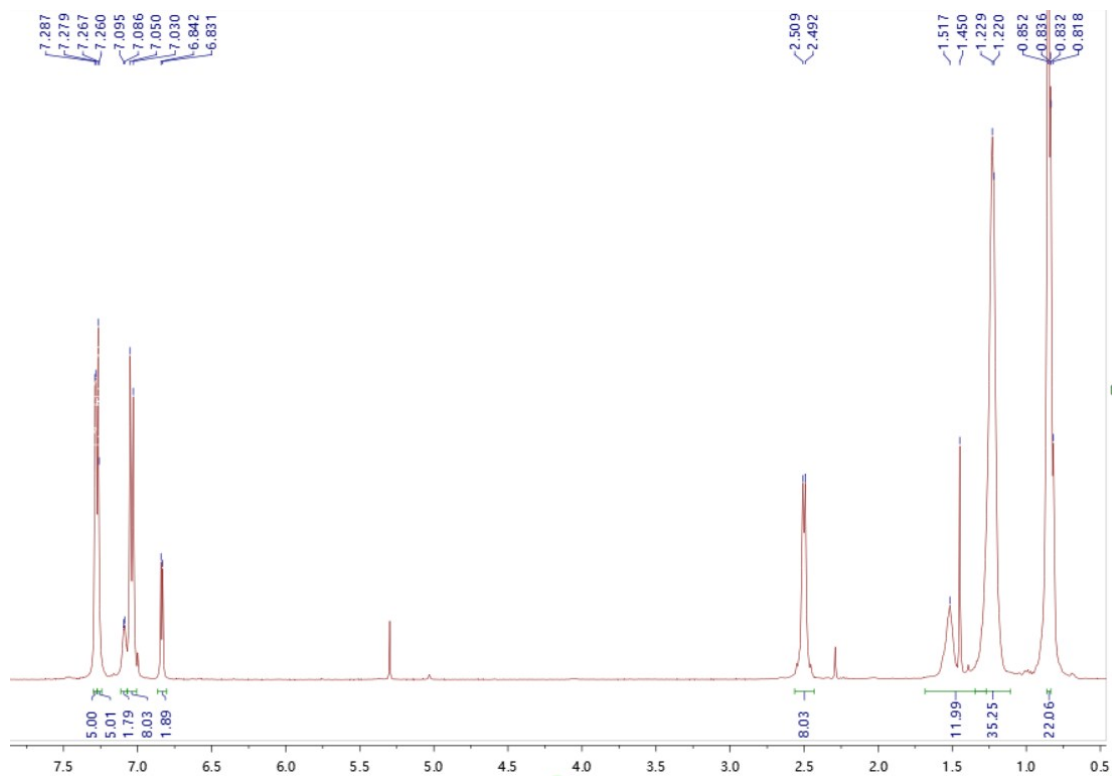


Figure S4. ^1H NMR of Compound 5

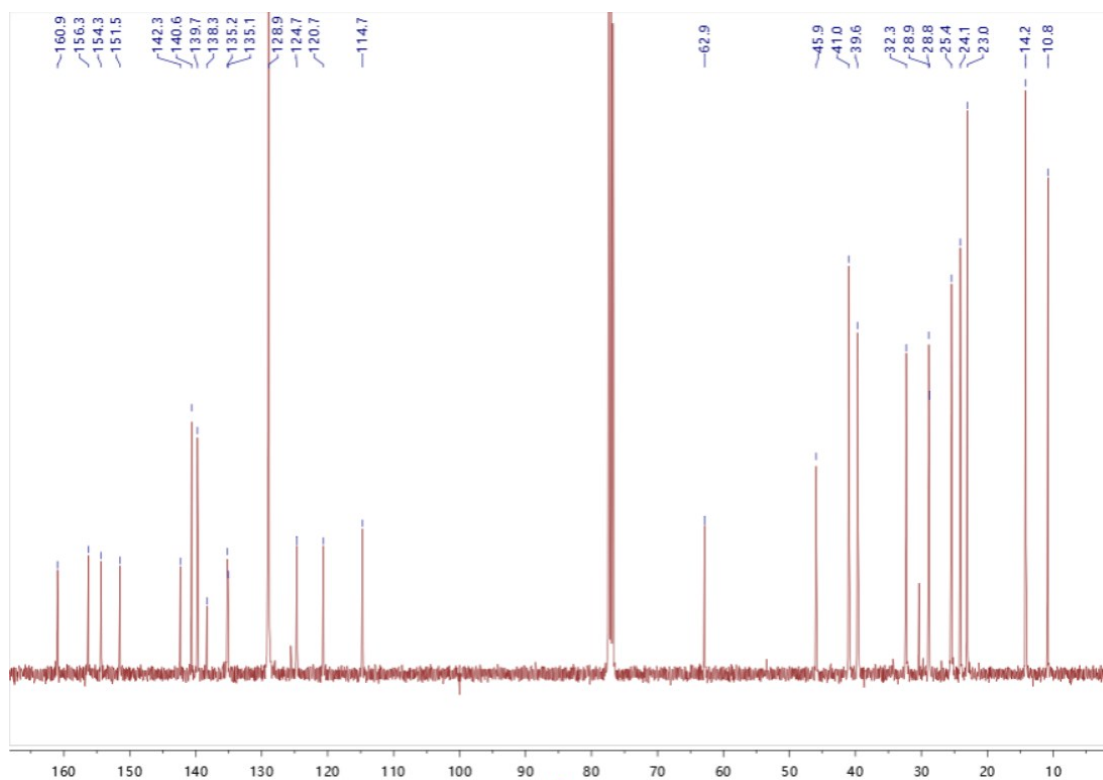


Figure S5. ^{13}C NMR of Compound 5

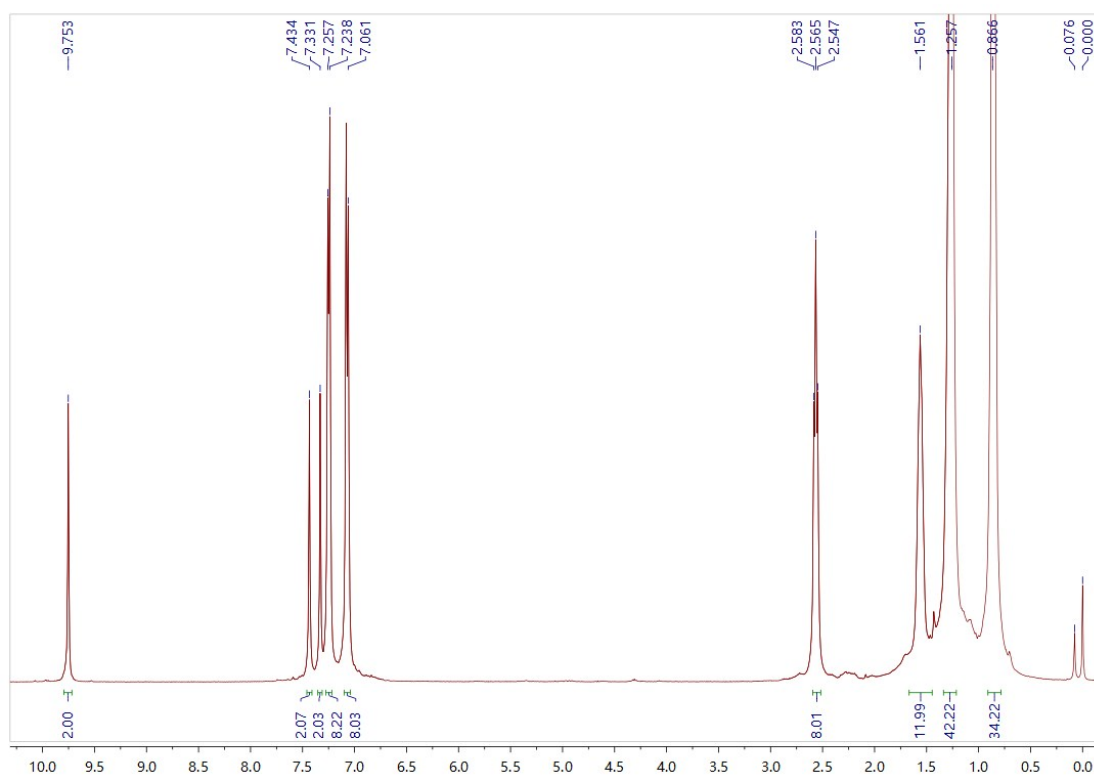


Figure S6. ^1H NMR of Compound 6

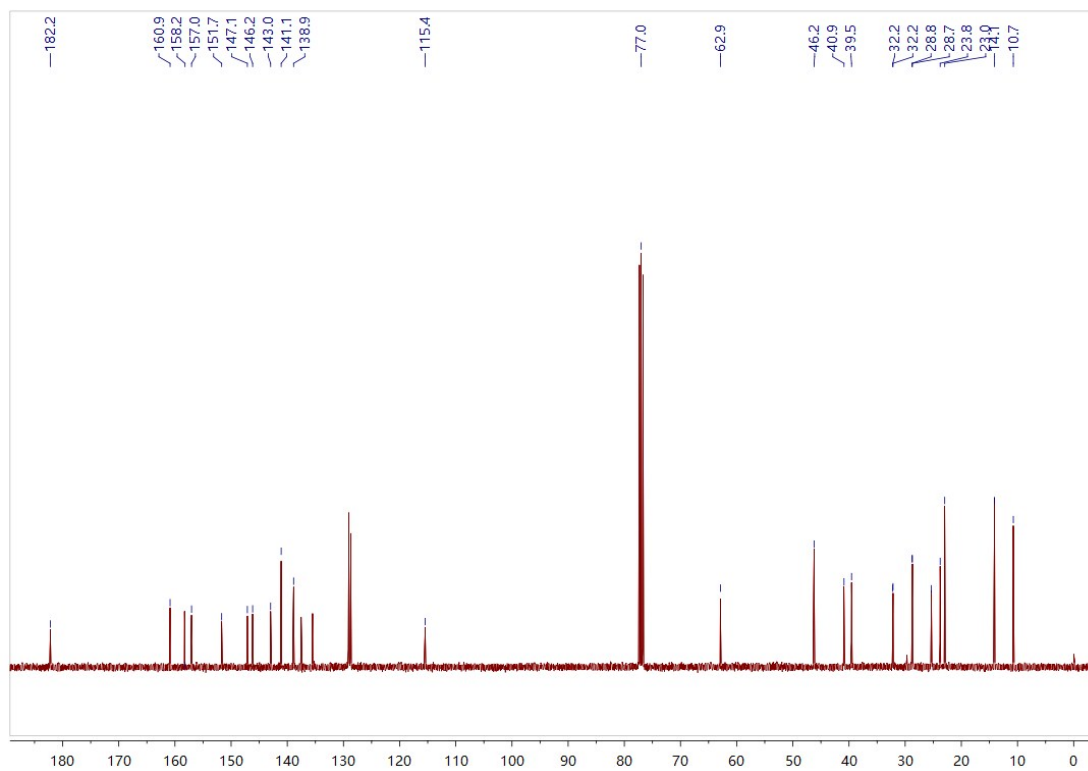


Figure S7. ^{13}C NMR of Compound 6

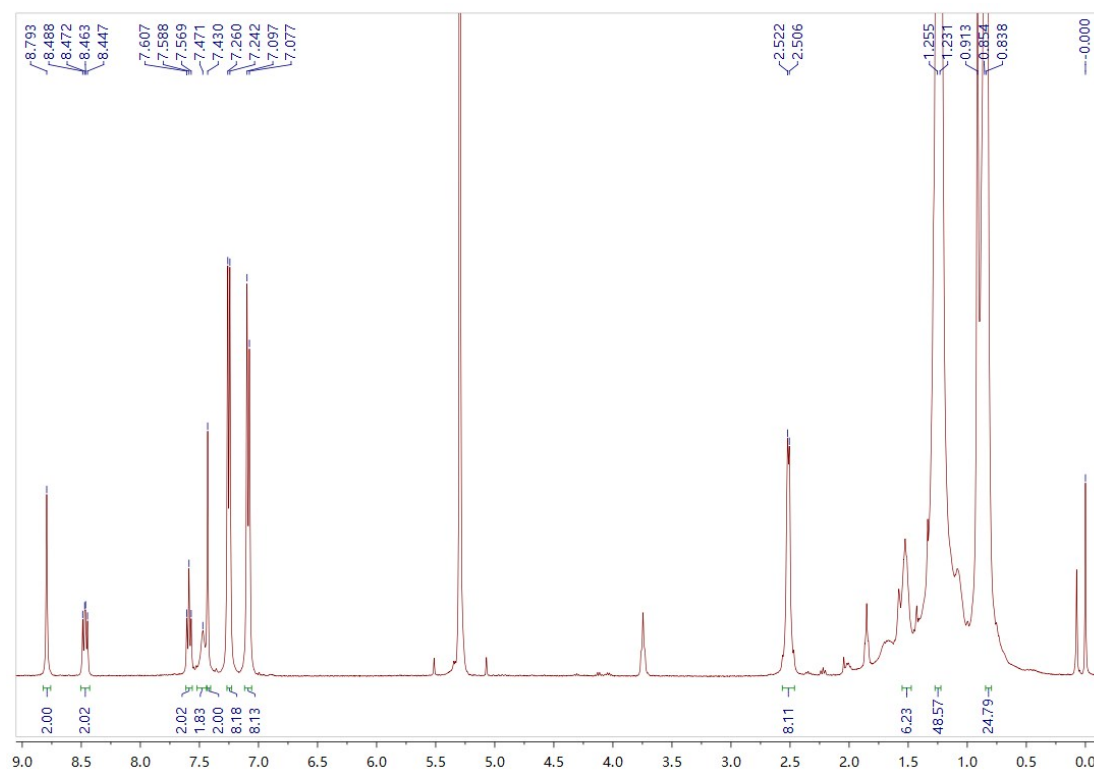


Figure S8. ^1H NMR of BCPT-4F

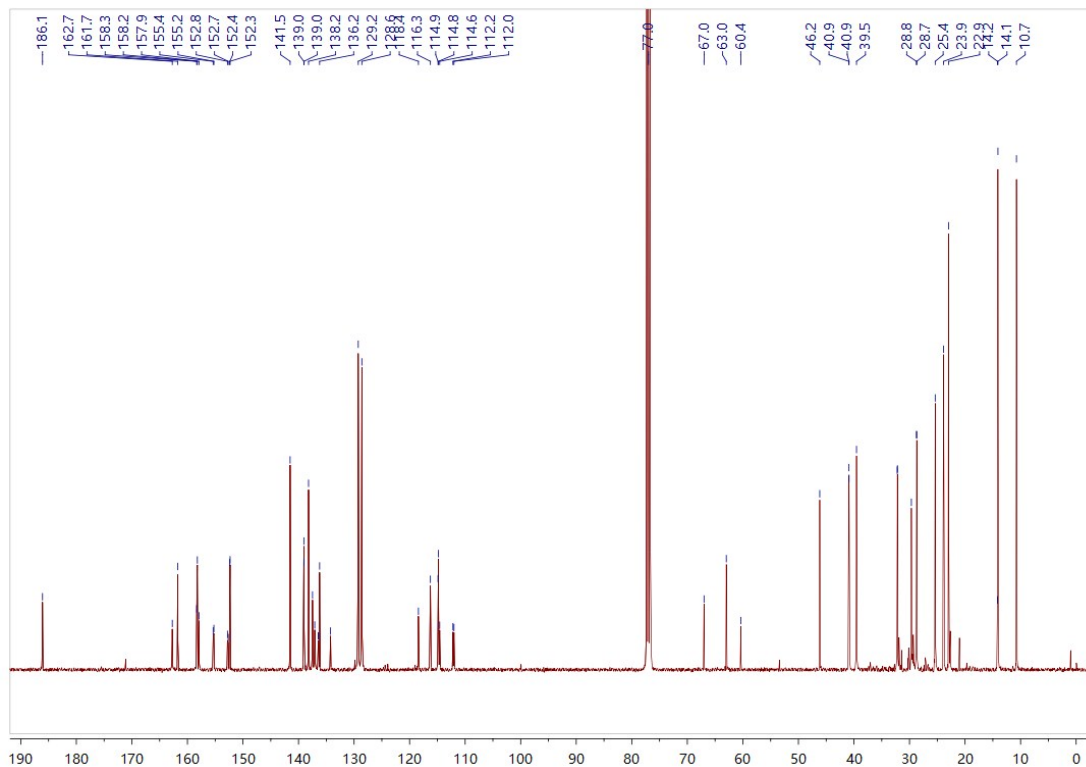


Figure S9. ^{13}C NMR of BCPT-4F

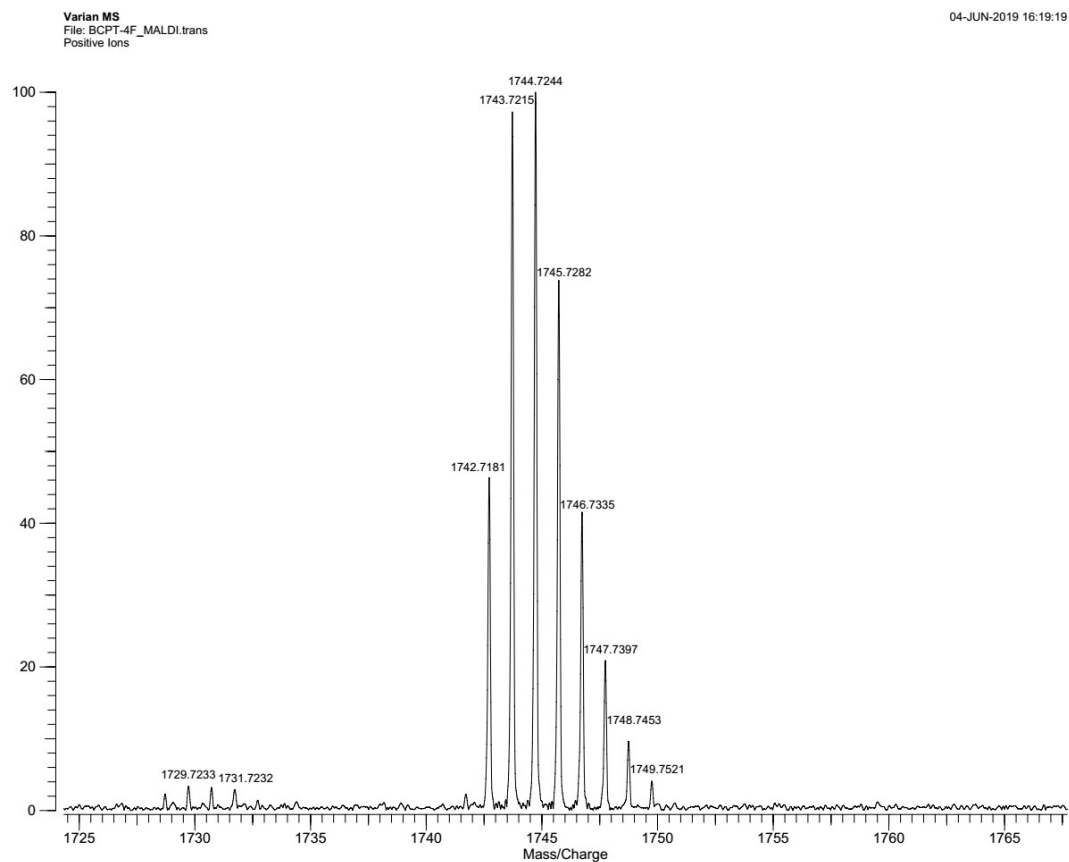


Figure S10. HR-FTMS of BCPT-4F

4. TGA Analysis and UV Absorption

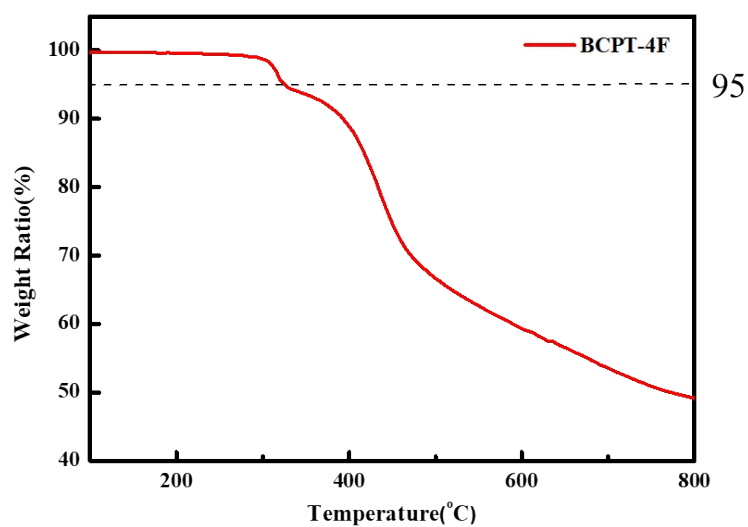


Figure S11. TGA curve of BCPT-4F with a heating rate of 10 °C/min

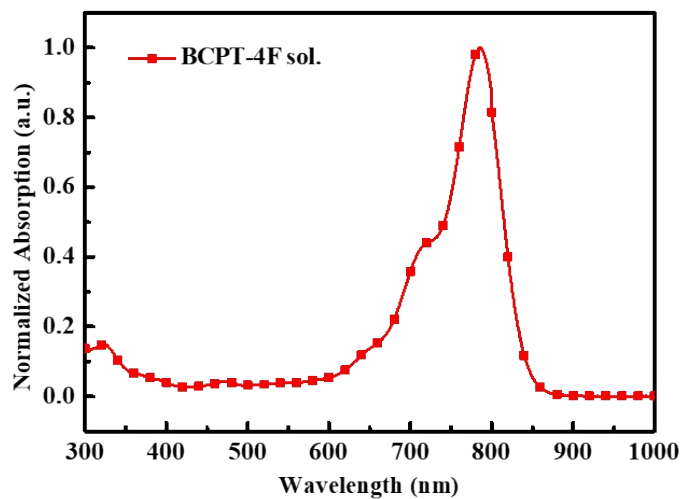


Figure S12. Normalized UV-Vis absorption spectrum of BCPT-4F in chloroform solution.

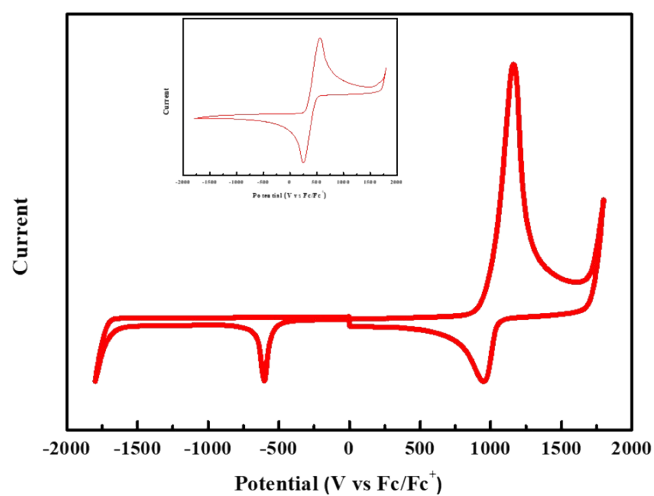


Figure S13. Electrochemical curve of BCPT-4F. Insert is the CV curve of FeCp₂.

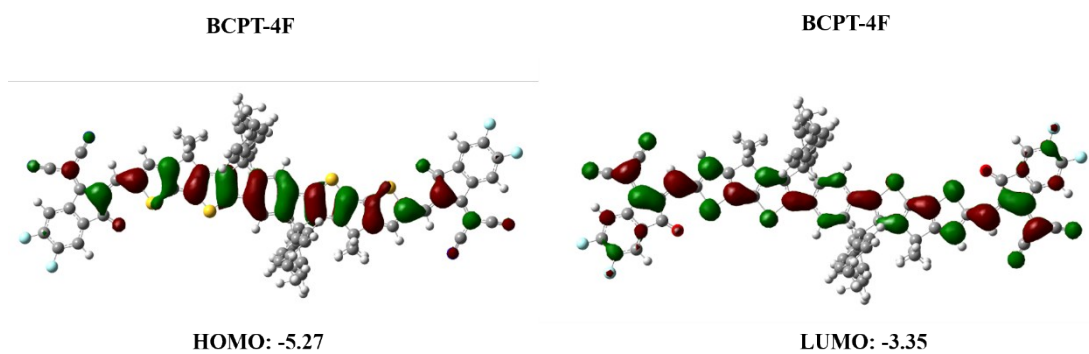


Figure S14. Theoretical density distribution for the frontier molecular orbitals via DFT-based theoretical calculations at the B3LYP/6-31G* level.

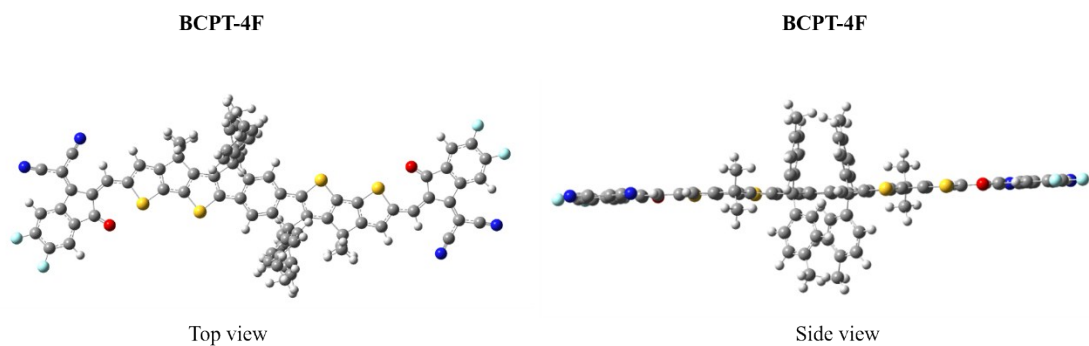


Figure S15. Optimized geometries of BCPT-4F using Gauss View calculations.

5. Device Fabrication and Measurements

The photovoltaic devices were fabricated with inverted structure of indium tin oxide (ITO)/ZnO/PFN-Br/PBDB-T:NFA/MoO_x/Ag. The current density-voltage (J - V) curves of photovoltaic devices were obtained by a Keithley 2400 source-measure unit. The photocurrent was measured under AM 1.5G illumination at 100 mW/cm² irradiation using a Enli SS-F5-3A solar simulator, calibrated with a standard Si solar cell (made by Enli Technology Co., Ltd., Taiwan, and calibrated report can be traced to NREL). The EQE spectrum was measured using a QE-R Solar Cell Spectral Response Measurement System (Enli Technology Co., Ltd., Taiwan). The hole and electron mobility were measured using the space charge limited current (SCLC) method, employing a diode configuration of ITO/PEDOT:PSS/active layer/Au for hole and glass/ZnO/active layer/Al for electron by taking the dark current density in the range of 0–8 V and fitting the results to a space charge limited form, where SCLC is described by

$$J = \frac{9\varepsilon_0\varepsilon_r\mu_0V^2}{8L^3} \exp\left(0.89\beta\sqrt{\frac{V}{L}}\right)$$

where J is the current density, L is the film thickness of the active layer, μ is the hole or electron mobility, ε_r is the relative dielectric constant of the transport medium, ε_0 is the permittivity of free space (8.85×10^{-12} F m⁻¹), V ($=V_{\text{appl}} - V_{\text{bi}}$) is the internal voltage in the device, where V_{appl} is the applied voltage to the device and V_{bi} is the built-in voltage due to the relative work function difference of the two electrodes.

Table S1. Photovoltaic performance of the solar cells based on PBDB-T:BCPT-4F with different D:A ratio under illumination of AM 1.5 G, 100 mW cm⁻².

D:A	V _{oc} (V)	FF	J _{sc} (mA cm ⁻²)	PCE (%)
1:0.8	0.78	0.68	21.15	11.18
1:1	0.78	0.65	22.16	11.33
1:1.2	0.78	0.63	22.12	10.92

Table S2. Photovoltaic performance of the solar cells based on PBDB-T:BCPT-4F (1:1, w/w) blend films with DIO additive under illumination of AM 1.5 G, 100 mW cm^{-2} .

V%	V_{oc} (V)	FF	J_{sc} (mA cm⁻²)	PCE(%)
None	0.78	0.65	22.16	11.33
0.2	0.78	0.68	22.44	11.87
0.3	0.78	0.70	22.96	12.43
0.4	0.78	0.69	21.44	11.54
0.5	0.77	0.70	21.29	11.47

Table S3. Photovoltaic performance of ternary solar cells with different ratios under illumination of AM 1.5 G, 100 mW cm^{-2} . PBDB-T:BCPT-4F:F-Br = D:A₁:A₂.

D:A₁:A₂	V_{oc} (V)	FF	J_{sc} (mA cm⁻²)	PCE(%)
1:1:0	0.78	0.70	22.96	12.43
1:0.7:0.3	0.78	0.70	23.84	12.94
1:0.5:0.5	0.81	0.71	24.88	14.23
1:0.3:0.7	0.81	0.71	22.57	13.04
1;0:1	0.86	0.74	18.05	11.52

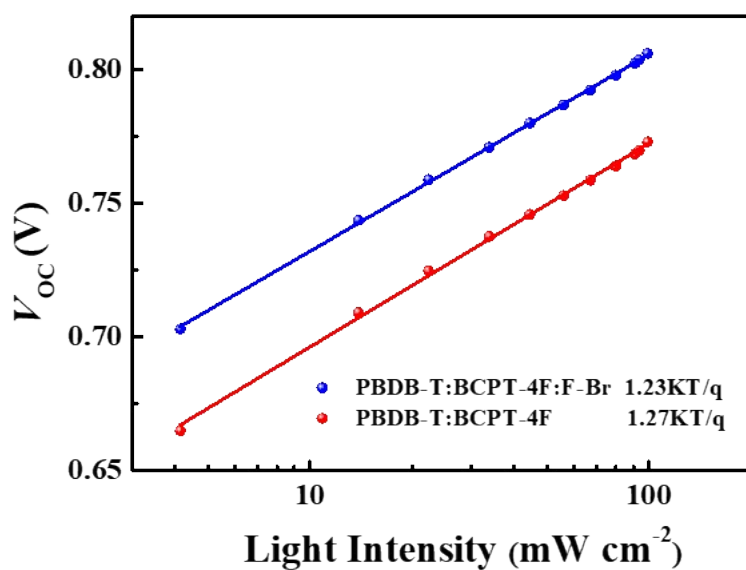


Figure S16. Light-intensity (P) dependence of V_{oc} measurement of the devices.

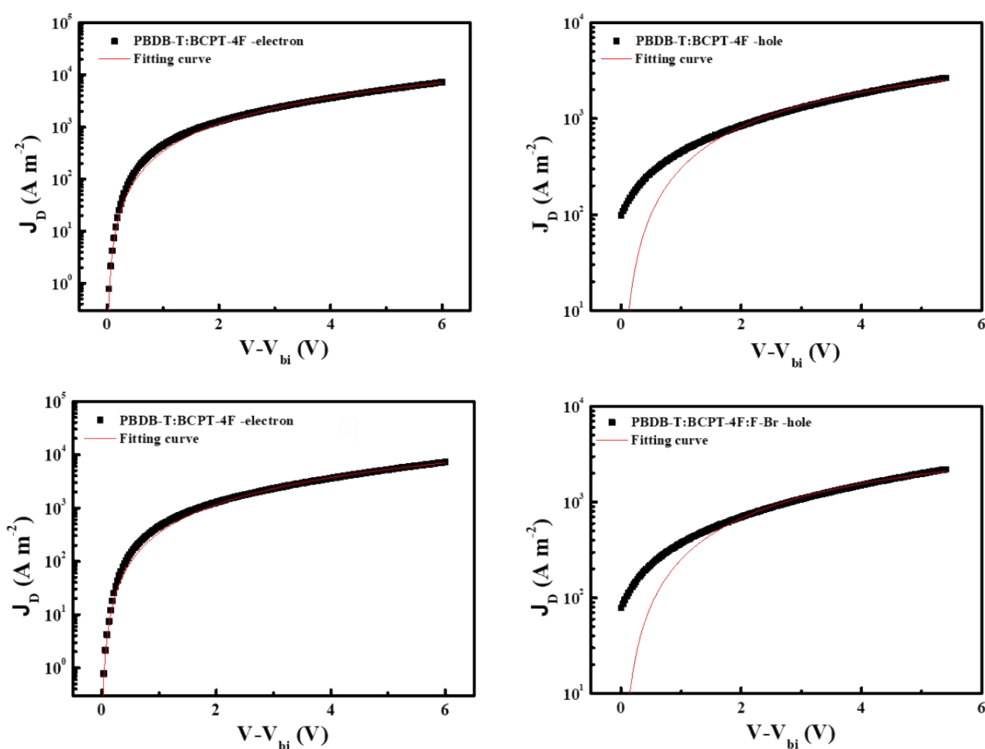


Figure S17. Plots for electron and hole mobilities based on PBDB-T:BCPT-4F and PBDB-T:BCPT-4F:F-Br=1:0.5:0.5 films. The solid lines represent the fit using a model of single carrier SCLC with field-independent mobility.

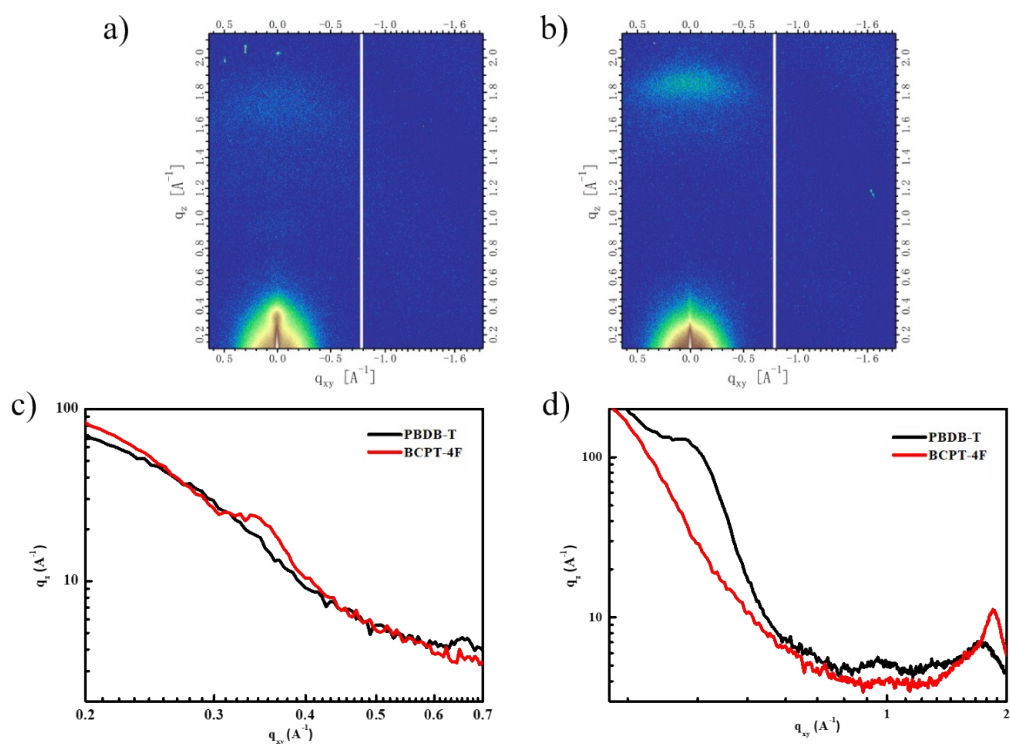


Figure S18. GIWAXS patterns for a) PBDB-T neat film and b) BCPT-4F neat film, and in-plane c) and out-of-plane line d) cuts of the corresponding GIWAXS patterns.

Table S3. Summary of photovoltaic parameters of CPT based-solar cells

D:A	V_{oc} (V)	FF(%)	J_{sc} (mA cm^{-2})	PCE(%)	Ref.
RD6:PC ₇₁ BM	0.85	53	8.25	3.72	1
PBDB-T:DOC6-IC	0.91	60.11	19.21	10.52	2
PBDB-T:DOC8-IC	0.92	57.65	17.74	9.41	2
PBDB-T:DOC2C6-IC	0.93	63.33	18.85	11.10	2
PBDB-T:DC6-IC	0.99	62.21	11.19	6.87	2
PBDB-T:DOC2C6-2F	0.85	73.15	21.35	13.24	2
PBDB-T:ITDI	0.94	59.78	13.94	7.82	3
PBDB-T:CDTDI	0.86	37.36	7.89	2.54	3
VC89:PC ₇₁ BM	0.92	62	11.68	6.66	4
PBDB-T:DF-PCIC	0.91	72	15.66	10.12	5
PTQ10:DF-PCIC	1.04	54.13	6.51	3.68	6
PTQ10:HC-PCIC	0.94	67.96	15.99	10.42	6
PBDB-TF:HC-PCIC	0.89	72.06	18.13	11.60	6
PBDB-T:FO-PCIC	0.90	61.12	15.02	8.32	6
PBDB-TF:HF-PCIC	0.91	70.77	17.81	11.49	7
PBDB-TF:HFO-PCIC	0.93	70.99	12.62	8.36	7
PBDB-TF:OF-PCIC	0.91	73.37	13.76	9.09	7
PBDB-T:DF-TCIC	0.86	58	16.39	8.23	8
PBDB-T:HF-TCIC	0.76	65	20.04	9.86	8

PTB7-Th:SSBR	0.92	55.83	15.91	8.16	9
PTB7-Th:SSBRC	0.77	56.33	7.75	3.35	9
PBDB-T:CPDT-4Cl	0.65	66.8	21.3	9.28	10
PBDB-T:CPDT-4F	0.68	69.6	20.1	9.47	10
P3HT:DFPCBR	0.80	64.39	10.39	5.34	11
PBDB-T:IDTC-4Cl:PC ₇₁ BM	0.829	65.6	19.14	10.41	12
PBDB-T:BDTC-4Cl:PC ₇₁ BM	0.856	67.2	21.19	12.19	13
PBDB-T:HF-PCIC:IEICO-4F	0.78	60.02	23.46	11.13	14
PBDB-TF:HC-PCIC:IT-M	0.88	73.82	18.69	12.34	15
PTB7-Th:CPDT-(TIC) ₂	0.838	46.4	14.81	5.76	16
PBDB-T:NOC6F-1	0.95	65.79	17.08	10.62	17
PBDB-T;NOC6F-2	0.96	53.26	13.21	6.74	17

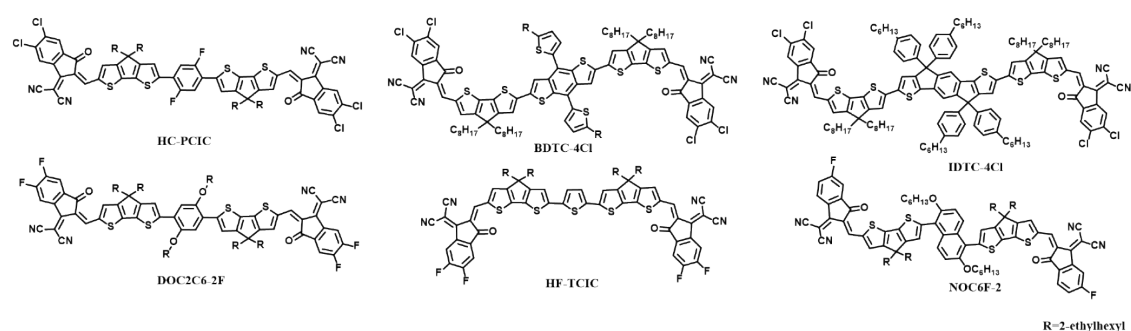


Figure S19. Structure of some classic CPT based non-fused ring molecules

6. References

1. R. Domínguez, N. F. Montcada, P. de la Cruz, E. Palomares and F. Langa, *Physical Chemistry Chemical Physics*, 2017, 19, 3640-3648.
2. H. Huang, Q. Guo, S. Feng, C. e. Zhang, Z. Bi, W. Xue, J. Yang, J. Song, C. Li, X. Xu, Z. Tang, W. Ma and Z. Bo, *Nature Communications*, 2019, 10, 3038.
3. Z. Kang, S.-C. Chen, Y. Ma, J. Wang and Q. Zheng, *ACS Applied Materials & Interfaces*, 2017, 9, 24771-24777.
4. C. V. Kumar, L. Cabau, A. Viterisi, S. Biswas, G. D. Sharma and E. Palomares, *The Journal of Physical Chemistry C*, 2015, 119, 20871-20879.
5. S. Li, L. Zhan, F. Liu, J. Ren, M. Shi, C.-Z. Li, T. P. Russell and H. Chen, *Advanced Materials*, 2018, 30, 1705208.
6. S. Li, L. Zhan, C. Sun, H. Zhu, G. Zhou, W. Yang, M. Shi, C.-Z. Li, J. Hou, Y. Li and H. Chen, *Journal of the American Chemical Society*, 2019, 141, 3073-3082.

7. S. Li, L. Zhan, W. Zhao, S. Zhang, B. Ali, Z. Fu, T.-K. Lau, X. Lu, M. Shi, C.-Z. Li, J. Hou and H. Chen, *Journal of Materials Chemistry A*, 2018, 6, 12132-12141.
8. R. Qin, W. Yang, S. Li, T.-K. Lau, Z. Yu, Z. Liu, M. Shi, X. Lu, C.-Z. Li and H. Chen, *Materials Chemistry Frontiers*, 2019, 3, 513-519.
9. C. Tang, S.-C. Chen, Y. Tang, W. Ma and Q. Zheng, *Solar Energy*, 2018, 174, 991-998.
10. K. Wang, J. Lv, T. Duan, Z. Li, Q. Yang, J. Fu, W. Meng, T. Xu, Z. Xiao, Z. Kan, K. Sun and S. Lu, *ACS Applied Materials & Interfaces*, 2019, 11, 6717-6723.
11. N. Wang, W. Yang, S. Li, M. Shi, T.-K. Lau, X. Lu, R. Shikler, C.-Z. Li and H. Chen, *Chinese Chemical Letters*, 2019, 30, 1277-1281.
12. Y.-Q.-Q. Yi, H. Feng, X. Ke, J. Yan, M. Chang, X. Wan, C. Li and Y. Chen, *Journal of Materials Chemistry C*, 2019, 7, 4013-4019.
13. Y.-Q.-Q. Yi, H. Feng, N. Zheng, X. Ke, B. Kan, M. Chang, Z. Xie, X. Wan, C. Li and Y. Chen, *Chemistry of Materials*, 2019, 31, 904-911.
14. L. Zhan, S. Li, H. Zhang, F. Gao, T.-K. Lau, X. Lu, D. Sun, P. Wang, M. Shi, C.-Z. Li and H. Chen, *Advanced Science*, 2018, 5, 1800755.
15. L. Zhan, S. Li, S. Zhang, T.-K. Lau, T. R. Andersen, X. Lu, M. Shi, C.-Z. Li, G. Li and H. Chen, *Solar RRL*, 2019, 3, 1900317.
16. Y. Zhang, X. Liu, H. Gu, L. Yan, H. Tan, C.-Q. Ma and Y. Lin, *Organic Electronics*, 2019, DOI: <https://doi.org/10.1016/j.orgel.2019.105530>, 105530.
17. R. Zheng, Q. Guo, D. Hao, C. e. Zhang, W. Xue, H. Huang, C. Li, W. Ma and Z. Bo, *Journal of Materials Chemistry C*, 2019, 7, 15141-15147.